Predicting Ejections of Compact Multi-Planet Systems

Chau Truong
Department of Physics, Princeton University

Advisor: Adam Burrows

Abstract

NASA's *Kepler* mission has discovered numerous multi-planet systems since its launch in 2006, many of which have been notable for their compact configurations with tightly packed planets on close orbits. These systems have become the focus of intense numerical investigations to gain insight into their long-term stability and evolution. In this study, we utilize the open-source code `REBOUND` to conduct N-body integrations to simulate the evolution of various compact multi-planet systems, ranging from those composed of five Earth-mass planets to ten Earth-mass planets and ten Jupiter-mass planets. Our primary objective is to explore the potential for planetary ejections within these systems and identify any discernible patterns. To do so, we analyze trends observed in the semi-major axis and eccentricity of each planet in each system over time. Our endeavors aim to deepen our understanding of compact multi-planet systems and their dynamics, offering valuable insights into their long-term evolution.

This paper represents my own work in accordance with University regulations.

/s/ Chau Truong

1 Introduction

Launched on March 6, 2009, NASA's *Kepler* mission had the primary objectives of detecting transiting exoplanets and determining the frequency of Earth-sized planets in the habitable zone (HZ) of solar-like stars [1] [2]. Since its launch, the mission has discovered hundreds of multi-planet systems [3] [4] [5]. Particularly noteworthy of these are compact systems whose planets are tightly packed and are on close orbits [3] [6]. An exemplary case is Kepler-11, with five of its six known planets orbiting within Mercury's semi-major axis, and the sixth planet orbiting just slightly beyond [7]. Similar systems include Kepler-33 [8], Kepler-32 [9], Kepler-80 [10], and Kepler-444 [11], all harboring five planets on close orbits. The discovery of these compact multi-planet systems has inspired many numerical investigations into their orbital stability. These studies yield crucial insights into the systems' formation and long-term evolution, shedding light on the processes that govern their existence.

Most previous works have focused on analyzing the stability of multi-planet systems within the framework of the Hill Problem, which considers the limiting case of the three-body problem, where two small planets orbit a much more massive central star, in which the orbital separation between the two planets becomes sufficiently small [12]. Generally, the mutual gravitational attraction between the two planets can be neglected, and the problem can be reduced to a superposition of two independent two-body problems. However, when planets' orbital separation becomes sufficiently small, the mutual attraction between them can no longer be ignored, as it increases to the same order as the gravitational attraction from the massive central star [12] [13]. In this case, strong interactions will occur between the two planets, resulting in a highly complex and chaotic evolution [14]. Exploring the general three-body problem in 1982, Marchal and Bozis realized that for certain initial conditions, conservation of energy and angular momentum will prevent close encounters between planets to occur for all time [15]. These systems are deemed "Hill stable" [16]. Although the definition of a "close encounter" varies between studies, it generally relies on considerations of the planets' spheres of gravitational influence. The sphere of gravitational influence is the region around a planet in which it is feasible to view the planet as the central body and the central star as the perturbing body [16] [17]. While there are different spheres of influence, the one that is particularly relevant in defining a close encounter is the Hill sphere.

The Hill sphere, whose derivation was motivated by the study of the tidal theory, is defined as the region around a planet within which the planet's gravity is the dominating force [17]. The size of this region is denoted by the Hill radius, the distance from the center of the planet to the outer boundary of the Hill sphere, given by

$$R_H = a\left[\frac{m}{3M}\right]^{1/3}, \tag{1}$$

where m is the planet mass, a is the semi-major axis of the planet's orbit, and M is the mass of the central star [17]. Generally, as a planet's mass increases, its Hill radius also increases.

The Hill problem can therefore be explained in terms of the planets' Hill spheres. When orbital separations between adjacent planets become small, their Hill spheres may begin to overlap, leading to increased gravitational interactions between the planets and perturbations in their orbits. Over time, this can cause a system to become unstable. In order to maintain

Hill stability, each planet must remain within only its own Hill sphere. Most studies of the orbital stability of multi-planet systems aim to gradually decrease the initial orbital separation between adjacent planets and determine the point at which the system cease being Hill stable. This criterion is referred to as the Hill stability limit, and it represents the minimum orbital spacing required for systems to avoid close encounters [18]. Examples of some of these studies are discussed in Section 2.

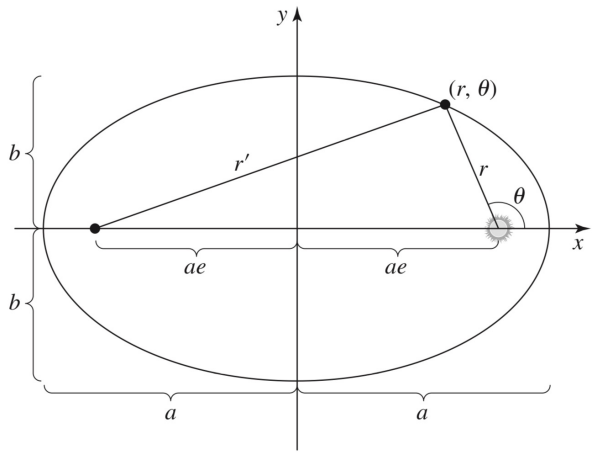

Figure 1: An ellipse of semi-major axis a and semi-minor axis b representing a planetary orbit with the central star at one focus from Ryden and Peterson [19].

In the long-term evolution of compact multi-planet systems, the ejection of a planet is a potential occurrence. To explore this phenomenon, we first need to review the defining characteristics of a Keplerian orbit.

The gravitational attraction between two bodies is described by Newton's law of universal gravitation

$$F = -\frac{GMm}{R^2}, \tag{2}$$

where G is the gravitational constant, M and m are the masses of the two bodies, and R is the distance separating them. Newton had derived the mathematical form of his law by requiring that the force of gravity F result in planetary orbits that obey Kepler's three laws of planetary motion [19].

Kepler's first law states that a planetary orbit take the shape of an ellipse, with the central star at one focus, depicted in Figure 1 [19]. The eccentricity of the ellipse, defined as the distance between the two foci divided by the length of the major axis, is given by

$$e = \left(1 - \frac{b^2}{a^2}\right)^{1/2}, \tag{3}$$

where a is the semi-major axis, and b is the semi-minor axis [19].

Kepler's second law states that the rate at which the planet-star vector sweeps out area is constant [19]. This law describes the conservation of angular momentum of a planetary orbit, which is given by

$$L = m\sqrt{GMa(1-e^2)}, \tag{4}$$

where M is the mass of the central star, m is the planet mass, a is the semi-major axis of the orbit, and e is the orbital eccentricity [19].

Kepler's third and final law describes the relation between the orbital period P and the semi-major axis a of an orbit [19]:

$$P^2 = \frac{4\pi^2}{GM} a^3. \tag{5}$$

Using units of solar masses for M, AU for a, and years for P, this formula simplifies to

$$P^2 = \frac{a^3}{M}. \tag{6}$$

The orbital energy of a planet E is the sum of its kinetic energy K and its gravitational potential energy U [19]:

$$E = K + U \tag{7}$$

$$= \frac{1}{2}mv^2 - \frac{GM}{R} \tag{8}$$

$$E = -\frac{GMm}{2a} \tag{9}$$

It should be noted that Kepler's first law deals with closed orbits, in other words, orbits with eccentricity $e < 1$ that form closed curves, either ellipses and circles. However, the physics of gravitation permits open orbits as well, parabolic or hyperbolic orbits with $e \geq 1$. For closed, elliptical orbits, the planet m is gravitationally bound by the central star M, resulting in $K < |U|$ and $E < 0$ [19].

For this study, we will only consider planets on closed, elliptical orbits with $e < 1$. Consequently, any planetary with an orbital eccentricity $e \geq 1$ will be considered ejected.

In this study, we are motivated by the discovery of compact multi-planet systems and the existing body of research on their stability. Our objective is to analyze the Hill stability limit of these systems and explore the potential of planetary ejections. We begin this paper by reviewing pertinent findings from previous studies in Section 2, followed by a description of our methodology in Section 3. Section 4 presents our results and provides an analysis of observed trends. Finally, in Section 5, we offer our conclusions and discuss avenues for future research.

2 Previous Work

2.1 Two-Planet Systems

The study of multi-planet stability begins with the foundational three-body problem, where two planets orbit a central star. Marchal and Bozis first explored the general three-body problem in 1982, determining that certain initial conditions imposed on the system will prevent close encounters occurring for all time [15]. Their study was followed by Gladman's

focused examination in 1993 of two planets orbiting a much more massive star [16]. Specifically, Gladman studied the dynamics of two small planets orbiting a solar-mass star. His investigation revealed that for initially coplanar and circular planetary orbits, the two-planet system will be Hill stable if the outer planet has a semi-major axis of

$$a_2 > a_1(1 + \Delta_c), \tag{10}$$

where

$$\Delta_c = 2\sqrt{3}\left(\frac{m_1 + m_2}{3M}\right)^{1/3}, \tag{11}$$

and m_1 and m_2 are the masses of the planets, and M is the mass of the central star. In other words, he determined that in a two-planet system, the planets will avoid a close encounter if their initial fractional orbital separation exceeds the critical value Δ_c. In this work, a close encounter is defined as when the separation between the two planets is less than the size of the sphere of influence, which scales with $2(m/M)^{2/5}$, of the more massive planet [16].

2.2 Multi-Planet Systems

Building upon the works of Marchal and Bozis, as well as Gladman, numerous numerical investigations have been conducted with the aim of finding the Hill stability limit across diverse multi-planet systems [14] [20] [18] [21], with a great focus on compact systems [22] [23] [24].

In many of these studies, the initial orbital separation between adjacent planets in a system is measured in units of the planets' mutual Hill radii $R_{H_{i,i+1}}$. This parameter represents the gravitational influence between adjacent planets and is expressed as

$$R_{H_{i,i+1}} = \left[\frac{m_i + m_{i+1}}{3M}\right]^{1/3} \frac{a_i + a_{i+1}}{2}. \tag{12}$$

Here, $i = 1, ..., N-1$, with N denoting the total number of planets in the system. m_i and a_i represent the mass and semi-major axis of planet i, respectively [14]. Consequently, the orbital separation between adjacent planets can be iteratively calculated with

$$a_{i+1} = a_i + \Delta R_{H_{i,i+1}} = a_i + \Delta\left[\frac{m_i + m_{i+1}}{3M}\right]^{1/3} \frac{a_i + a_{i+1}}{2}, \tag{13}$$

where Δ is a specified multiple of $R_{H_{i,i+1}}$. For compact systems, $\Delta < 10$ [22]. In systems comprised of equal-mass planets, $m_i = m_{i+1}$, leaving

$$a_{i+1} = a_i + \Delta\left[\frac{2m}{3M}\right]^{1/3} \frac{a_i + a_{i+1}}{2}. \tag{14}$$

From this, the semi-major axis ratio between the orbits of adjacent planets can be obtained:

$$\frac{a_{i+1}}{a_i} = \left[1 + \frac{\Delta}{2}\left(\frac{2m}{3M}\right)^{1/3}\right]\left[1 - \frac{\Delta}{2}\left(\frac{2m}{3M}\right)^{1/3}\right]^{-1}. \tag{15}$$

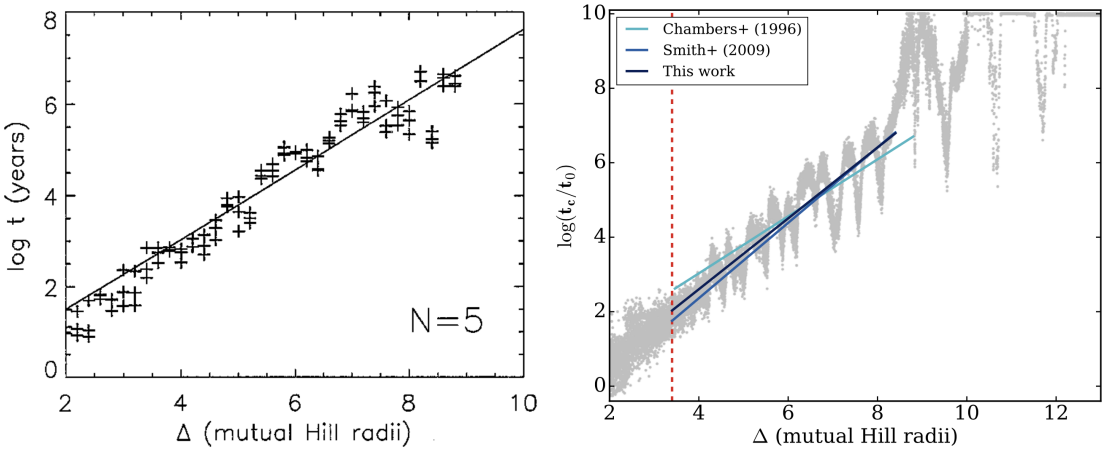

Figure 2: The logarithm of instability time t_{inst} as a function of initial orbital separation in mutual Hill radii Δ for five 10^{-7} $M_\odot$ planets on initially coplanar, circular orbits from Chambers *et al.* [14] (left). Fit is given in Figure 3. The logarithm of t_{inst} as a function of Δ for five Earth-mass planets on initially coplanar, circular orbits from Obertas *et al.* [23], with fits from Chambers *et al.* [14] and Smith and Lissauer, where $t_0 = 1$ AU is the initial orbital period of the innermost planet [22] (right). Fits are given in Figure 4.

N	b	c
3	1.176 ± 0.051	−1.663 ± 0.274
5	0.765 ± 0.030	−0.030 + 0.192
10	0.756 ± 0.027	−0.358 ± 0.176
20	0.757 ± 0.038	−0.508 ± 0.244

Figure 3: Least squares fit values for b and c in Equation 16 for systems with $N = 3,\ 5,\ 10,\ 20$ 10^{-7} $M_\odot$ planets from Chambers *et al.* [14].

Reference	b	c	range	μ_i
Chambers et al. (1996)	0.765	−0.030	$2\sqrt{3} < \Delta \leq 8.8$	10^{-7}
Smith and Lissauer (2009)	1.012	−1.686	$3.4 \leq \Delta \leq 8.4$	3.0035×10^{-6}
This work	0.951	−1.202	$\Delta_C < \Delta < 8.4$	3.0035×10^{-6}

Figure 4: Least squares fit values for b and c in Equation 16 for systems of five equal mass planets from Chambers *et al.* [14], Smith and Lissauer [22], and Obertas *et al.* [23]. Here, Δ_c represents the critical two-planet separation in units of the mutual Hill radius, and $\mu = m/M$ is the reduced mass of the planets in each system [23]. Figure obtained from Obertas *et al.* in [23].

It is important to note that this ratio reveals a non-uniform spacing of the planets' orbits, the outer planets have larger Hill radii compared to inner planets in a system [14].

In their work, Chambers *et al.* studied the orbital evolution of systems of three or more small planets orbiting around a solar-mass star [14]. Their exploration began with an investigation of three 10^{-7} $M_\odot$ planets in initially coplanar, circular orbits with the innermost

planet having a semi-major axis of $a_1 = 1$ astronomical unit (AU), and those of the second and third planets following Equation 13. In contrast to the results found by Gladman for the case of the two-planet system, where only systems with an initial fractional orbital separation less than the critical value Δ_c (Equation 11) are unstable [16], Chambers *et al.* found that a close encounter occurred between a pair of planets in almost all the three-planet systems, where they defined a close encounter as when two planets approached one another within one mutual Hill radius [14]. For systems where a close encounter did not occur by the end of the integrations, Chambers *et al.* predicted that these systems will eventually also go unstable on longer timescales [14]. They were able to derive a relationship between the time at which a system goes unstable, or experiences a close encounter, referred to as the instability time, t_{inst} and initial orbital separation in mutual Hill radii Δ. (It should be noted that different groups denote this instability time with different symbols. Chambers *et al.* uses t [14], Obertas *et al.* uses t_c [23], and Lammers *et al.* uses t_{inst} [24]. For consistency, we refer to this time where a system goes unstable as t_{inst}.) Specifically, Chambers *et al.* found that the instability time of a system of three planets on initially coplanar, circular orbits depend exponentially on initial orbital separation [14]. This relationship can be written in the form

$$\log_{10} t_{inst} = b\Delta + c, \tag{16}$$

where b and c are constants that depend on the number and masses of the planets [14]. Examining different planetary systems with varying number of planets and varying planet masses, Chambers *et al.* found that these systems share the same behavior [14]. An example is shown in Figure 2 (left), which depicts the logarithm of the instability time as a function of initial orbital separation in mutual Hill radii for five 10^{-7} $M_\odot$ planets, with the data gathered fitted to Equation 16. The least squares fit values for b and c are given in Figure 3 for various numbers of planets in a system N. Other studies have been able to reproduce the same findings [18] [20] [22] [23]. The relationship derived by Chambers *et al.* can subsequently be used to predict the timescale on which a system will undergo close encounters and collisions.

Beyond the three-planet systems, Chambers *et al.* also examined systems with varying number of planets and varying planet masses. Comparing systems of $N = 3,\ 5,\ 10,\ 20$ planets, they found that the instability time was reduced from the three-planet system to the five-planet system [14]. However, they found that increasing the number of planets beyond five did not significantly decrease the instability time of the system [14]. After performing integrations with varying planet masses, Chambers *et al.* concluded that normalizing orbital separations by a new factor of $\left(\frac{m}{M}\right)^{1/4}$ rather than $\left(\frac{m}{M}\right)^{1/3}$ better predicts instability times for a wider range of masses [14].

Further research has studied the impact of varying parameters on the instability time of planetary systems. Morrison and Kratter, for example, examined high-mass, multi-planet systems and found that trends from lower-mass planetary systems fail to predict instability times for these high-mass systems, by up to orders of magnitude for some orbital separations [18]. Wang *et al.* studied the influence of initial orbital inclinations on instability time, concluding that initial inclinations within $[0°,\ 10°]$ do not have significant effects on the instability time of massive multi-planet systems. Instead, they emphasized that orbital eccentricities are the dominant factor influencing the instability of these systems [21]. In addition to reproducing results obtained by Chambers *et al.* [14], Smith and Lissauer found

that for a system of five Earth-mass planets on initially coplanar, circular orbits around a central star, instability time increases more sharply for $\Delta > 8.4$ [22]. Their study also revealed that adding a widely-spaced Jupiter had small effects on the instability time of a system consisting of five Earth-mass planets [22]. Obertas *et al.* was also able to recover results of Chambers *et al.* [14] and Smith and Lissauer [22], and obtained a linear relationship between initial orbital spacing in mutual Hill radii and the logarithm of instability time. Fits from the three studies are compared in Figures 2 and 4. They also confirmed the claim of Smith and Lissauer in [22] that there is a sharp increase in instability time for $\Delta > 8.4$. Additionally, their simulations revealed sharp drops in instability times at certain initial orbital spacings, specifically near $\Delta \sim 9.5$, $\Delta \sim 10.6$, and $\Delta \sim 11.8$ [23].

Most recently, Lammers *et al.* also conducted simulations of systems of five Earth-masses orbiting around a solar-mass star [24]. Rather than measuring initial orbital separation in units of mutual Hill radii as preceding works have done, they chose to measure orbital separation between adjacent planets in terms of the planets' period ratio, where

$$\mathcal{P} = \frac{P_{i+1}}{P_i} = \left(\frac{a_{i+1}}{a_i}\right)^{3/2}. \tag{17}$$

For compact systems, $\mathcal{P} \lesssim 1.5$ [24]. In their work, Lammers *et al.* developed simplified dynamical models for gravitational interactions in multi-planet systems and compared their predictions against the results of N-body simulations, with the objective of clarifying the underlying dynamical mechanism leading to orbital instabilities [24].

3 Methodology

The code used in this paper to perform the necessary simulations and numerical integrations is `REBOUND`, an open-source N-body code courtesy of Hanno Rein and Shang-Fei Liu [25] [26]. Originally released in 2011 exclusively in C, `REBOUND` has since introduced a Python version of the code [25] [26]. For this paper, we will be using the Python implementation of `REBOUND`.

3.1 `REBOUND`

`REBOUND`, akin to other N-body codes, simulates the dynamical evolution of systems consisting of multiple interacting particles under the influence of gravity. Particles in these simulations can represent stars, planets, moons, rings, or dust particles. A distinguishing feature of `REBOUND` in comparison to other N-body codes is its modularity. Users have the flexibility to combine different gravity solvers, collision detection algorithms, boundary conditions, and integration methods based on the specific requirements of their projects. Since its initial release in 2011, `REBOUND` has undergone significant enhancements. As of 2024, it offers five gravity solvers, four collision detection algorithms, and eleven integration methods [26].

`REBOUND` uses direct summation to calculate the gravitational forces between all particle pairs in a system and more specifically, the acceleration onto each particle [25] [26]. For the

ith particle in a system, this is given by

$$\overrightarrow{a_i} = \sum_{j=0}^{N_{active}-1} \frac{Gm_j}{(r_{ij}^2 + b^2)^{3/2}} \hat{r}_{ji}, \tag{18}$$

where G is the gravitational constant, m_j is the mass of the jth particle, and $\overrightarrow{r_{ji}}$ is the relative distance between particles j and i [25].

As mentioned previously, `REBOUND` offers eleven numerical integrators to evolve particles forward in time, one timestep at a time [26]. The motion of particles in a system is described by a set of ordinary differential equations, the equations of motion. Each integrator approximates the true solution of the equations of motion numerically, determining the position and velocity of each particle over time, iterating in successive timesteps. Each integrator performs these calculations differently. Consequently, each of them has advantages and disadvantages [26]. The integrators offered by `REBOUND` include `IAS15` [27], `WHFast` [28], `MERCURIUS` [29], the standard leap frog integrator, and many others [26].

Finally, `REBOUND` is able to handle collisions and close encounters, making it ideal for this study of the instability times of planetary systems. `REBOUND` offers users four collision detection modules, each of which will check for instantaneous overlaps between every pair of particles either at the end of each timestep, during the timestep, or during the last timestep [26].

The two primary objects in `REBOUND` are the Simulation and Particle objects. The Simulation object contains all the configuration, status and particle data of one `REBOUND` simulation [26]. The Particle object represents one particle in a simulation and contains variables describing its mass, physical radius, position, and velocity [26]. When adding particles to a simulation, `REBOUND` allows users to adjust the particles' orbital parameters, including the semi-major axis of their orbit a, the eccentricity e, the inclination angle i, and many others as illustrated in Figure 5 [26]. After particles have been added to a simulation, `REBOUND` provides users with a method to plot the instantaneous orbits of the created system, as depicted in Figure 6 [26].

By default, `REBOUND` simulations use units in which $G = 1$ [26]. For a simulation with a central body of mass $M = 1$ and a test particle orbiting on a circular orbit at a distance $a = 1$, the orbital period of the test particle is given by

$$P = 2\pi\sqrt{\frac{a^3}{GM}} = 2\pi. \tag{19}$$

Here, $M = 1$ corresponds to one solar mass and $a = 1$ corresponds to one AU. Thus, $P = 2\pi$ corresponds to one year in these units [26]. The Python implementation of `REBOUND` includes a set of functions that allows the users to change the system of units for a simulation [26]. For example, users can choose to use meters, kilograms, and seconds to measure distance, mass, and time, respectively. They can also choose to use AU, solar masses, and years instead, or combinations of these units.

The versatility of `REBOUND`, demonstrated by its different modules and customizable orbital parameters, and its ability to handle collisions and close encounters makes it an excellent tool for investigating the instability times of various planetary systems.

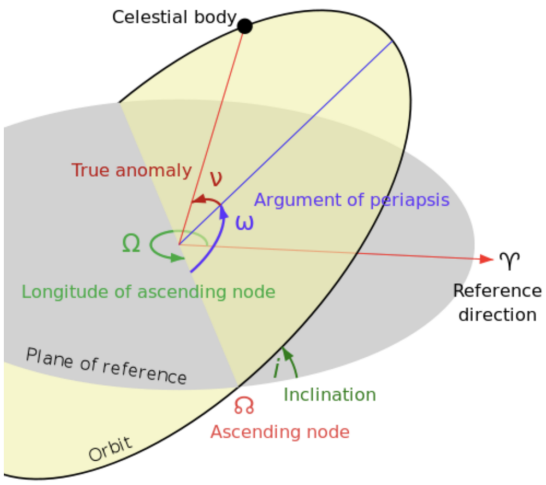

Figure 5: An illustration of the most important angles used as orbital parameters in `REBOUND` from [26].

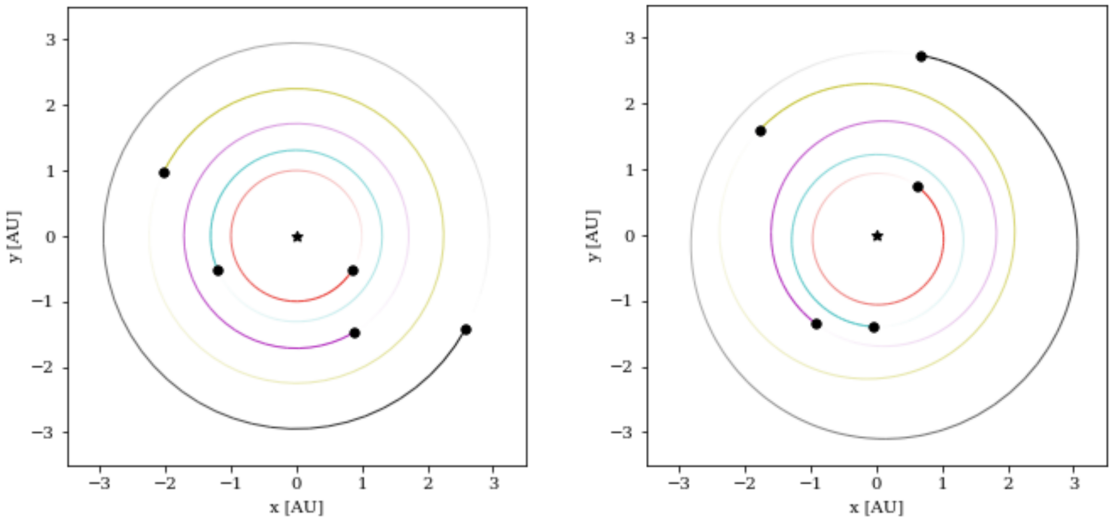

Figure 6: Visualizing the instantaneous orbits of planetary systems using `OrbitPlot` in `REBOUND` for systems with planets on initially circular (left) and initially eccentric (right) orbits [25]. Plots were created from simulations of systems consisting of five planets with initial orbital separations sharing a common period ratio $\mathcal{P} = 1.5$. A normalized eccentricity $e_i/e_{cross} = 0.50$ was used for the `OrbitPlot` depicting initially eccentric orbits (right).

3.2 N-Body Simulations

Following the work of Lammers *et al.*, we conducted simulations of planetary systems consisting of planets on initially coplanar orbits around a solar-mass star, assigning initial orbital separations such that adjacent planet pairs share a common period ratio $\mathcal{P}$ (Equation 17) [24]. For an ensemble of simulations, the common period ratio $\mathcal{P}$ was drawn uniformly from an interval $[\mathcal{P}_{min}, \mathcal{P}_{max}]$, where the lower and upper limits were chosen by trial-and-error such

that instability times for a system range from $\sim P_1$ to $\sim 10^7 P_1$ and P_1 is the initial orbital period of the innermost planet [24]. Following Chambers *et al.* [14], Smith and Lissauer [22], and Obertas *et al.* [23], we set the semi-major axis of the innermost planet to be $a_1 = 1$ AU to ensure that it completes one revolution around the central star in one year $P_1 = 1$ yr. Just as Lammers *et al.* had done, we assigned the planets' orbital eccentricities based on their system's period ratio spacing [24]. We set the eccentricities to be a constant fraction of the orbit-crossing eccentricity

$$e_{cross}(\mathcal{P}) = \frac{\mathcal{P}^{2/3} - 1}{\mathcal{P}^{2/3} + 1}, \tag{20}$$

where the orbit-crossing eccentricity is defined such that if adjacent planets in a system share a common period ratio $\mathcal{P}$ and have eccentricities $e = e_{cross}$, their orbits can overlap [24]. Finally, the planets' initial mean longitudes and longitudes of periapsis were randomly drawn from $[0, 2\pi)$.

Our simulations were conducted with `REBOUND` using the Wisdom-Holman integrator `WHFast` [28] with units of AU, solar mass $M_\odot$, and years. For all simulations, integrations used a timestep of $P_1/20$ and continued until a total time of 10^7 P_1, or 10 million years, passed.

We first generated ensembles of simulations of systems consisting of five Earth-mass planets ($M \sim 3 \cdot 10^{-6}$ $M_\odot$) with four normalized eccentricites $e_i/e_{cross} \in \{0.00, 0.25, 0.50, 0.75\}$, resulting in a total of four ensembles. The first three of the four normalized eccentricities are consistent with those used by Lammers *et al.* [24]. For these systems, the instability time t_{inst} was recorded when a pair of planets' orbits first overlapped, or when

$$(1 - e_{i+1})a_{i+1} - (1 + e_i)a_i < d, \tag{21}$$

where d is the Hill radius of the innermost planet as defined by Equation 1. For systems with a normalized eccentricity of $e_i/e_{cross} = 0.00$, the semi-major axis a and orbital eccentricity e for each planet was also recorded for each timestep.

We also generated two additional ensembles of simulations, this time of systems consisting of ten Earth-mass planets and systems consisting of ten Jupiter-mass planets ($M \sim 318$ $M_\oplus$) with a normalized eccentricity of $e_i/e_{cross} = 0.00$. Just as before, we recorded the semi-major axis a and orbital eccentricity e for each planet for each timestep.

4 Results

4.1 Systems of 5 Earth Masses

Figures 7, 8, and 9 shows the results of our N-body integrations for systems consisting of five Earth-mass planets.

In Figure 7, each panel depicts the instability time t_{inst} as a function of initial period ratio $\mathcal{P}$ for a normalized eccentricity in $e_i/e_{cross} \in \{0.00, 0.25, 0.50, 0.75\}$. We confirm the claims of Chambers *et al.* [14], Smith and Lissauer [22], Obertas *et al.* [22], and Lammers *et al.* [24] that instability times scale with initial orbital separation according to a power law. We also confirm the claim of Lammers *et al.* [24] that instability times decrease with

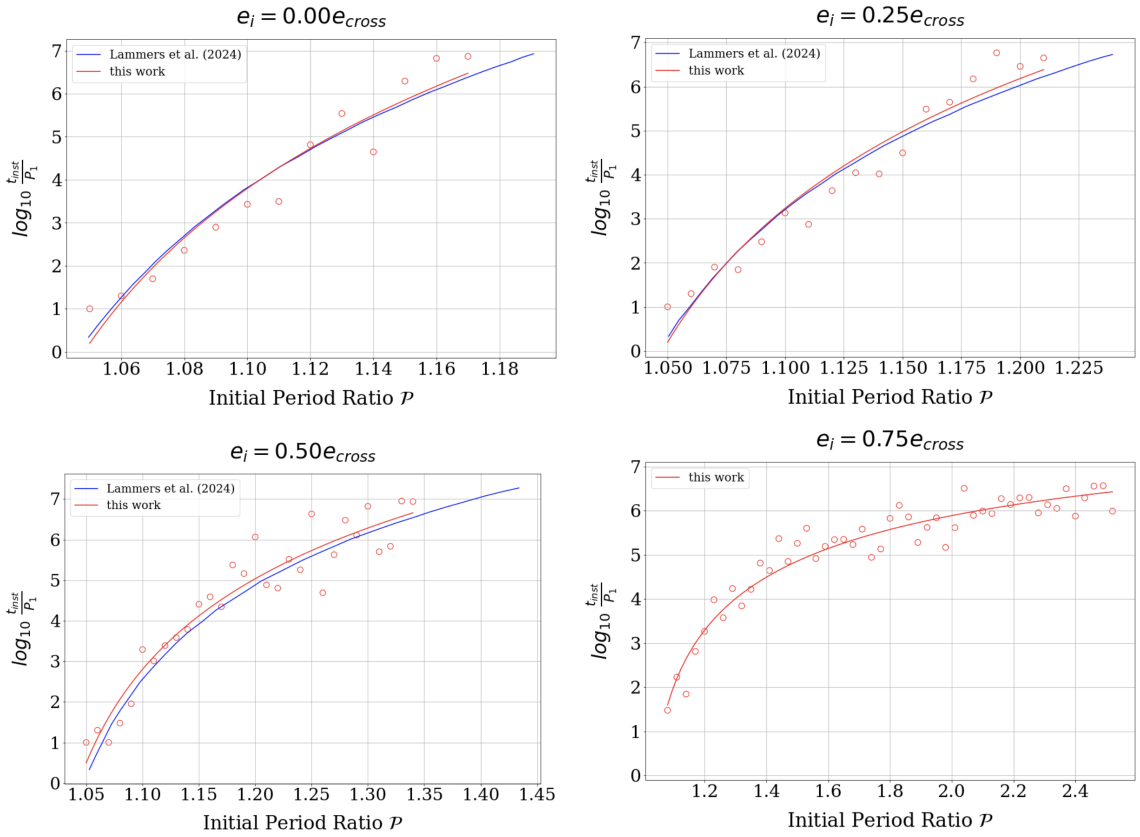

Figure 7: The logarithm of instability time t_{inst} as a function of period ratio $\mathcal{P}$ for planetary systems of five Earth-mass planets with normal eccentricities of $e_i/e_{cross} = 0.00$, $e_i/e_{cross} = 0.25$, $e_i/e_{cross} = 0.50$, and $e_i/e_{cross} = 0.75$. For the plots corresponding to systems with normalized eccentricities of $e_i/e_{cross} \in 0.00,\ 0.25,\ 0.50$, empirical fits (Equation 22) from Lammers *et al.* [24] are overlaid.

increasing normalized eccentricities of the planets. Lammers *et al.* observed this trend using normalized eccentricities $e_i/e_{cross} \in \{0.00, 0.25, 0.50\}$ [24], and we were able to see this trend continue with $e_i/e_{cross} = 0.75$ in the bottom right panel of Figure 7. More specifically, we observe that for a period ratio $\mathcal{P} = 1.20$, the logarithm of the instability time $\log_{10}(t_{inst}/P_1)$ decrease across the panels from $\log_{10}(t_{inst}/P_1) > 7$ for $e_i/e_{cross} = 0.00$ to $\log_{10}(t_{inst}/P_1) \sim 3$ for $e_i/e_{cross} = 0.75$.

We used the following function adopted by Lammers *et al.* to perform an empirical fit over our data in each panel:

$$\log_{10}\frac{t_{inst}}{P_1} = \left(A + B\left(\frac{e_i}{e_{cross}}\right)\right)\log_{10}\left[\frac{a_{i+1}-a_i}{a_{i+1}+a_i}\left(\frac{M_*}{m}\right)^{1/4}\right] + C + D\left(\frac{e_i}{e_{cross}}\right), \tag{22}$$

where A, B, C, and D are free parameters [24]. Using Equation 17, we find

$$\frac{a_{i+1}-a_i}{a_{i+1}+a_i} = \frac{\frac{a_{i+1}}{a_i}-1}{\frac{a_{i+1}}{a_i}+1} = \frac{\mathcal{P}^{2/3}-1}{\mathcal{P}^{2/3}+1}. \tag{23}$$

Therefore, the empirical fit function adopted by Lammers *et al.* can be rewritten as

$$\log_{10}\frac{t_{inst}}{P_1} = \left(A + B\left(\frac{e_i}{e_{cross}}\right)\right)\log_{10}\left[\frac{\mathcal{P}^{2/3}-1}{\mathcal{P}^{2/3}+1}\left(\frac{M_*}{m}\right)^{1/4}\right] + C + D\left(\frac{e_i}{e_{cross}}\right). \tag{24}$$

It is important to note the factor of $(m_i/M_*)^{-1/4}$ in spacing units, chosen based on the results from the study done by Chambers *et al.* [14], discussed in Section 2. In their work, Lammers *et al.* performed a least-squares fit and found $A = 11.9$, $B = -7.67$, $C = 5.20$, and $D = -3.26$. Our fits for ensembles with normalized eccentricities $e_i/e_{cross} \in \{0.00, 0.25, 0.50\}$ are compared to that from Lammers *et al.* in Figure 7.

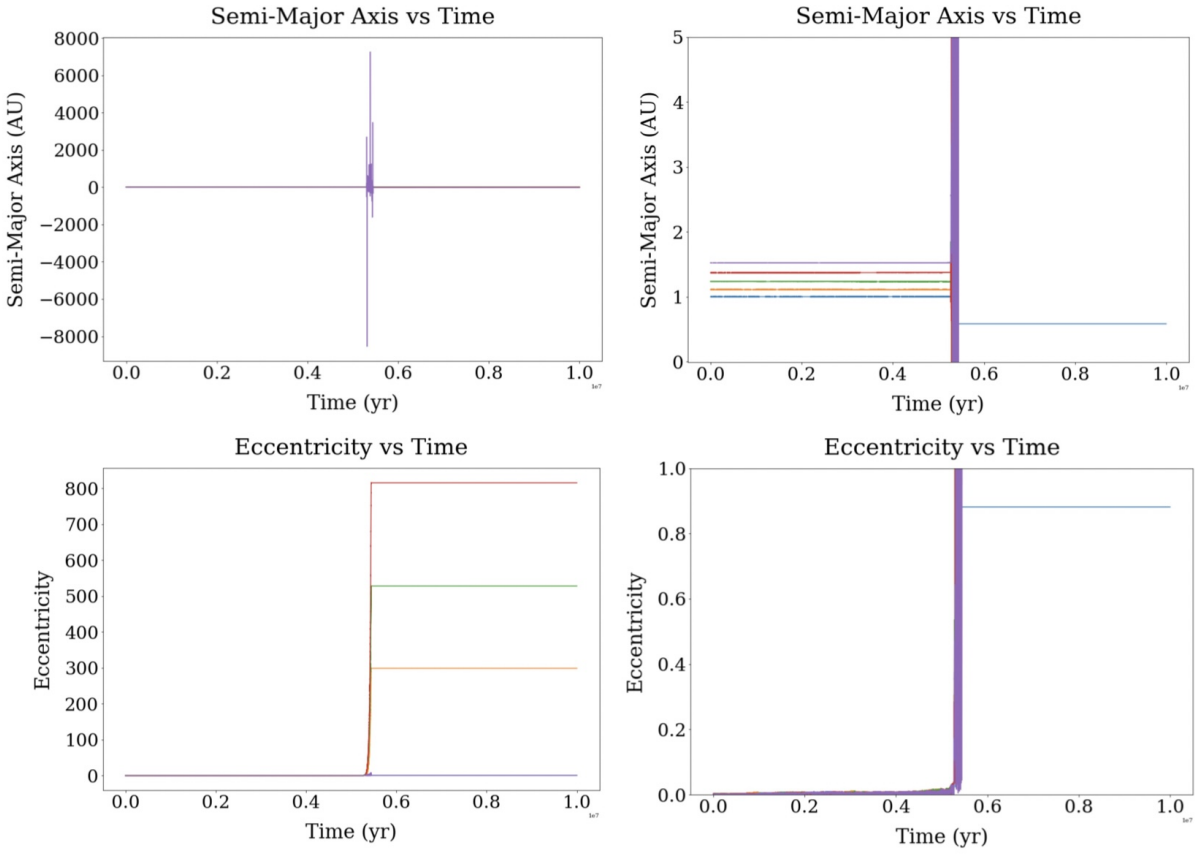

Figure 8: Semi-major axis a versus time (top row) and orbital eccentricity versus time (bottom row) for a simulation consisting of five Earth-mass planets with initial orbital separation following a common period ratio $\mathcal{P} = 1.17$. An enlarged view of each plot is provided (right column).

In Figures 8 and 9, we plot the semi-major axis a and orbital eccentricity e of each planet over the duration of the integrations for period ratios $\mathcal{P} = 1.17$ and $\mathcal{P} = 1.14$, respectively. In the right column of both figures, we present an enlarged view of each plot. From both figures, it can be observed that a and e begin to exhibit unstable behavior at the same point in time. To be more precise, we characterize "unstable behavior" as when the lines representing the semi-major axis a of each planet spike to zero or negative values and when

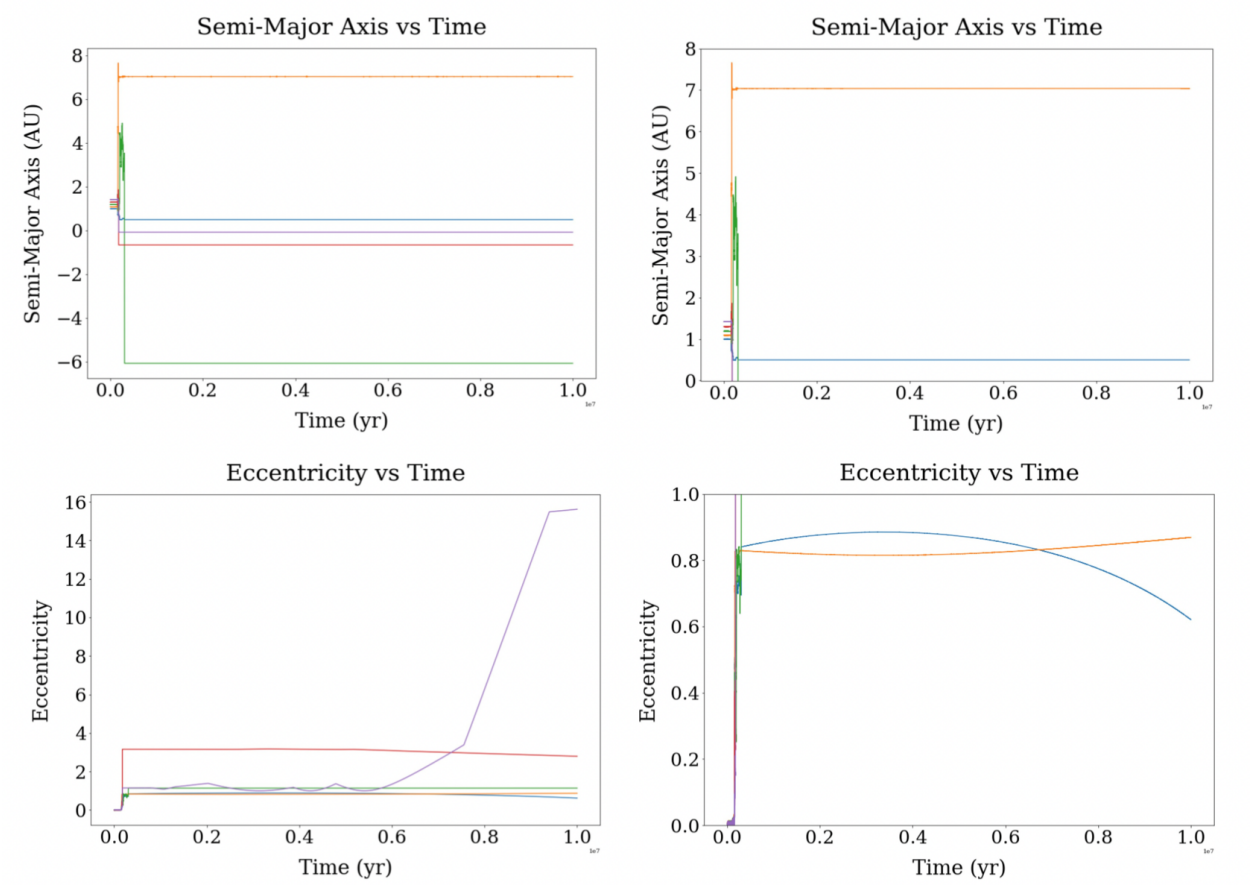

Figure 9: Semi-major axis a versus time (top row) and orbital eccentricity versus time (bottom row) for a simulation consisting of five Earth-mass planets with initial orbital separation following a common period ratio $\mathcal{P} = 1.14$. An enlarged view of each plot is provided (right column).

those representing the orbital eccentricity e of each planet spike to values greater than or equal to one. We see in the figures that a and e for all planets remain constant until a time t when the lines begin to suddenly spike. For the simulation in Figure 8 using a period ratio of $\mathcal{P} = 1.17$, this point in time occurs around $t \sim 5.35 \cdot 10^6$ years, and for the simulation in Figure 9 using a period ratio of $\mathcal{P} = 1.14$, it occurs around $t \sim 1.65 \cdot 10^5$ years. This also validates our previous observation from Figure 7 that smaller initial orbital separation decreases instability time. It should be noted that the time at which the semi-major axes and orbital eccentricities of the planets exhibit unstable behavior, which we denote as t, is different than the instability time t_{inst} that has been the variable of interest thus far. t_{inst} refers to the time at which a pair of planets' orbits overlap for the first time during the integrations, expressed mathematically in Equation 21, which does not necessarily occur at the same time at which a and e of the planets go unstable t.

For the ensemble of simulations for a system consisting of five Earth-mass planets, simulations were ran for period ratios beginning with $\mathcal{P} = 1.05$ and ending with $\mathcal{P} = 1.18$ in

increments of $\Delta\mathcal{P} = 0.01$. For the simulation using $\mathcal{P} = 1.18$, the system remains stable within the total integration time of 10^7 P_1. For most other simulations ran, all five planets are ejected within the integration time. In other words, by the end of the integrations at a time 10^7 P_1, no planet has an orbital eccentricity $e < 1$. A few systems are exceptions, such as those using a period ratio in $\mathcal{P} \in \{1.05,\ 1.09,\ 1.14,\ 1.17\}$. For systems using period ratios in $\mathcal{P} \in \{1.05,\ 1.09,\ 1.17\}$, only the innermost planet remains in the system by the end of the integrations. For these systems, we observe that after the semi-major axes and eccentricities of all the planets exhibit unstable behavior at a time t, those of the innermost planet stabilize to a constant value for the rest of the integration time. This can be seen for the simulation using $\mathcal{P} = 1.17$ in the enlarged plots of Figure 8, where the semi-major axis and eccentricity of the innermost planet stabilizes to $a \sim 0.60$ AU and $e \sim 0.90$. For the simulation using $\mathcal{P} = 1.09$, the semi-major axis and eccentricity of the planet that remains stabilizes to $a \sim 4$ AU and $e \sim 0.85$, respectively, and those of the planet that remains in the simulation using $\mathcal{P} = 1.05$ stabilizes to $a \sim 0.75$ AU and $e \sim 0.4$.

A notable case is the simulation using a period ratio of $\mathcal{P} = 1.14$, whose results are showcased in Figure 9, where the *two* innermost planets remain in the system by the end of the integrations. We see that the semi-major axis of the innermost planet (blue curve) stabilizes to $a \sim 0.5$ AU and that of the second innermost planet (orange curve) stabilizes to $a \sim 7$ AU, resulting in a period ratio of $\mathcal{P} \sim 52$.

However, in contrast to the case of $\mathcal{P} = 1.17$ where the eccentricity of the planet that remains in the system also stabilizes to a constant value, the eccentricities of the two innermost planets that remain in the system for $\mathcal{P} = 1.14$ are not constant. For the innermost planet (blue curve), the eccentricity appears to be decreasing, whereas the eccentricity for the second innermost planet (orange curve) appears to be increasing. A potential direction for future work includes investigating the ultimate fate of this system, possibly by integrating on longer timescales to observe whether the eccentricities of the two planets stabilize to constant values.

4.2 Systems of 10 Earth Masses

Figures 10 and 11 shows the results of our N-body integrations for systems consisting of ten Earth-mass planets.

For the ensemble of simulations for a system consisting of ten Earth-mass planets, simulations were ran for period ratios beginning with $\mathcal{P} = 1.05$ and ending with $\mathcal{P} = 1.25$ in increments of $\Delta\mathcal{P} = 0.01$. For most simulations using $\mathcal{P} \geq 1.18$, the system remains stable within the total integration time of 10^7 P_1, with the exception of the simulation using $\mathcal{P} = 1.20$, where all ten planets are ejected.

For the majority of the simulations using a period ratio in $1.05 \leq \mathcal{P} \leq 1.17$, all ten planets are ejected by the end of the integrations as well. A remarkable scenario occurs in the simulation with $\mathcal{P} = 1.16$. In this simulation, although all ten planets are ejected, the two innermost planets are ejected at a noticeably later time than the other planets, contrasting the results of the other simulations, where all ten planets are ejected at similar times. This is depicted in the enlarged plots of Figure 10. In these plots, an initial spike of a and e for all planets occurs at $t \sim 3 \cdot 10^6$ years, but a second spike occurs for the two innermost planets at $t \sim 3.80 \cdot 10^6$ years, resulting in their ejection.

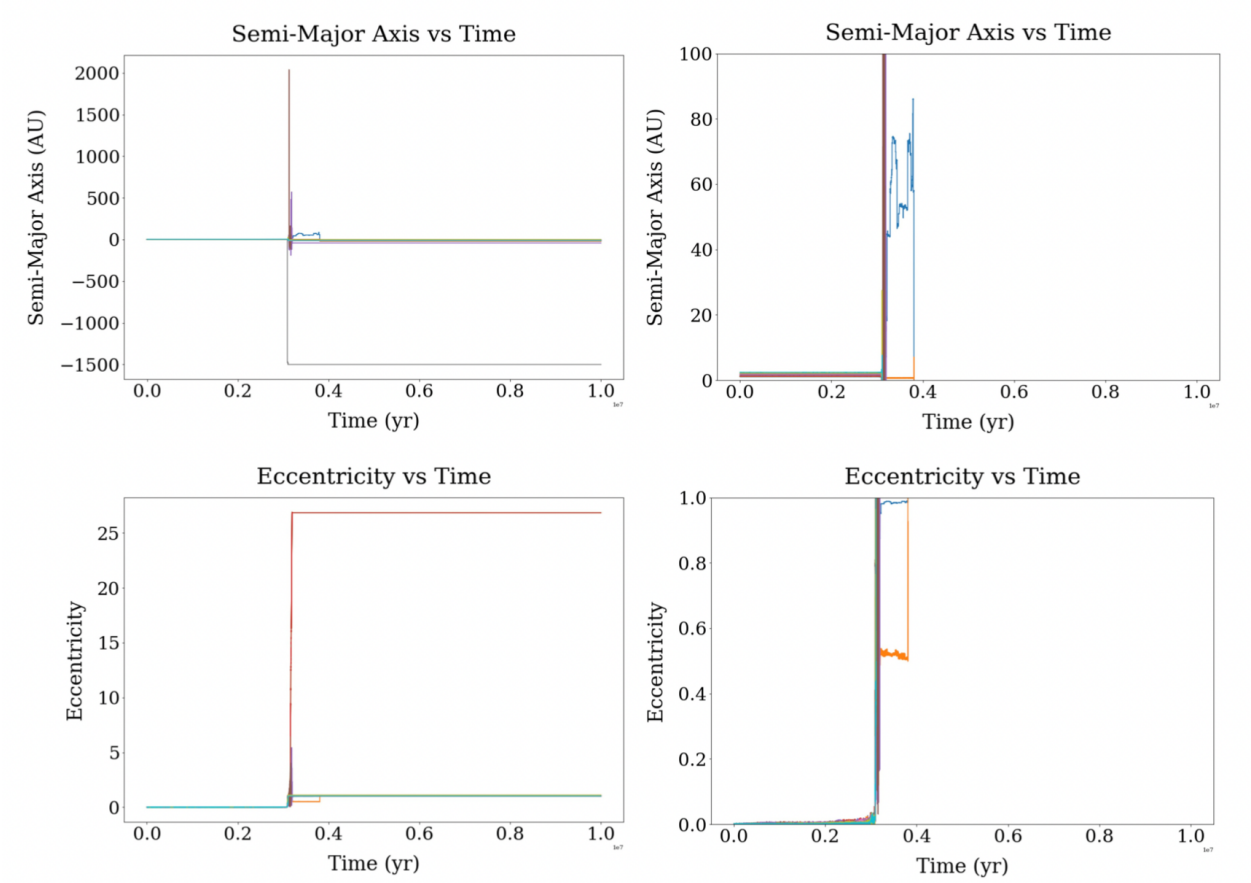

Figure 10: Semi-major axis a versus time (top row) and orbital eccentricity versus time (bottom row) for a simulation consisting of ten Earth-mass planets with initial orbital separation following a common period ratio $\mathcal{P} = 1.16$. An enlarged view of each plot is provided (right column).

For the other portion of these simulations, those using a period ratio in $\mathcal{P} \in \{1.09,\ 1.12,\ 1.13,\ 1.14\}$, one planet remains in the system, the innermost planet. Figure 11 displays a record of the stabilized semi-major axis a and eccentricity e of the remaining planet for each of such simulation. It is worth noting that the stabilized semi-major axis a of the remaining planets increase with increasing period ratio $\mathcal{P}$.

In an initial simulation of a system comprising ten Earth-mass planets with a period ratio of $\mathcal{P} = 1.07$, one planet, the innermost planet, had remained in the system with a stabilized semi-major axis and eccentricity of $a = 1.25$ AU and $e = 0.42$. However, upon repeating the integrations, it was observed that all ten planets were ejected from the system. No parameters were altered for the initial conditions of the system, with the exception of the initial mean longitude and longitude of periapsis of each, both of which were randomly drawn for each simulation. Future work could explore the influence of these parameters on planetary ejections.

$\mathcal{P}$	Stabilized a (in AU)	Stabilized e
1.09	0.4	0.91
1.12	0.75	0.2
1.13	1.350	0.55
1.14	1.550	0.2

Figure 11: The stabilized semi-major axis a and orbital eccentricity e of the singular remaining planet in simulations of systems consisting of ten Earth-mass planets with initial orbital separation following period ratios $\mathcal{P} \in \{1.07,\ 1.09,\ 1.12,\ 1.13,\ 1.14\}$.

4.3 Systems of 10 Jupiter Masses

Figures 12, 13, and 14 shows the results of our N-body integrations for systems consisting of ten Jupiter-mass planets.

For the ensemble of simulations for a system consisting of ten Jupiter-mass planets, simulations were ran with period ratios beginning with $\mathcal{P} = 1.20$ and ending with $\mathcal{P} = 3.05$ in increments of $\Delta\mathcal{P} = 0.05$.

For most simulations using a period ratio $2.10 \leq \mathcal{P} \leq 3.05$, the system remains stable by the end of the integrations at 10^7 P_1. Exceptions are the two systems using $\mathcal{P} = 2.50$ and $\mathcal{P} = 3.00$, where all planets with the exception of the innermost planet are ejected. For the simulation using $\mathcal{P} = 3.00$, the semi-major axis and eccentricity of the remaining planet stabilizes to $a \sim 5.7$ AU and $e \sim 0.92$. The simulation using $\mathcal{P} = 2.50$ presents an anomaly, as the eccentricity of the remaining planet appears to oscillate about $e \sim 0.92$, while its semi-major axis stabilizes at $a \sim 0.84$ AU. Results from this simulation are displayed in Figure 12.

For about half of the simulations of period ratios $1.20 \leq \mathcal{P} \leq 2.05$, all ten planets are ejected. For the other half of these simulations, specifically those with a period ratio in $\mathcal{P} \in \{1.20,\ 1.40,\ 1.55,\ 1.60,\ 1.65,\ 1.75,\ 1.90,\ 1.95\}$, only one planet remains by the end of the integrations. Figure 14 displays the stabilized semi-major axis a and eccentricity e of the remaining planet for each of the aforementioned simulation. Peculiar cases are those with a period ratio in $\mathcal{P} \in \{1.40,\ 1.60,\ 1.75,\ 1.95\}$. For $\mathcal{P} = 1.75$ and $\mathcal{P} = 1.95$, the eccentricity of the remaining planet oscillates about a value, listed in Figure 14 for each simulation, just as it did in the case with $\mathcal{P} = 2.50$ in Figure 12. For $\mathcal{P} = 1.40$, the eccentricity of the remaining planet does not stabilize to a constant value nor oscillate, while its semi-major axis stabilizes to $a \sim 1.1$ AU. For $\mathcal{P} = 1.60$, there is a small nudge in both the semi-major axis and the eccentricity of the remaining planet around $t \sim 6 \cdot 10^6$ years, depicted in Figure 13. After the nudge, a and e stabilize to constant values, with the eccentricity saturating to a value close to 1.

5 Conclusion

In this study, we conducted N-body integrations to simulate the evolution of various compact multi-planet systems, such as those comprised of five Earth-mass planets (Section 4.1), ten Earth-mass planets (Section 4.2), and ten Jupiter-mass planets (Section 4.3). Our sim-

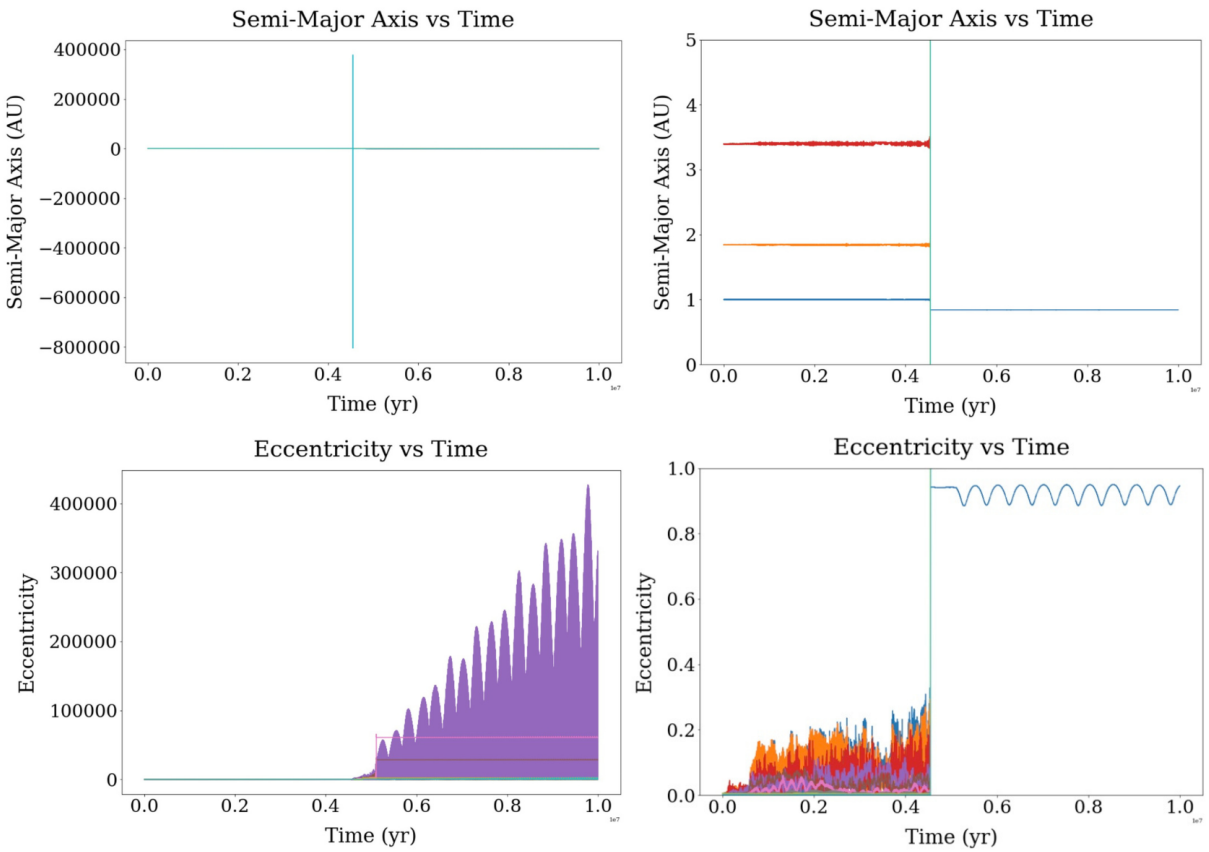

Figure 12: Semi-major axis a versus time (top row) and orbital eccentricity versus time (bottom row) for a simulation consisting of ten Jupiter-mass planets with initial orbital separation following a common period ratio $\mathcal{P} = 2.50$. An enlarged view of each plot is provided (right column). A notable feature is the oscillating e of the one planet remaining in the system (bottom right).

ulations were carried out using the open-source N-body code `REBOUND` by Hanno Rein and Shang-Fei Liu [25] [26], described in Section 3.1. Leveraging the capabilities of `REBOUND`, we were able to follow the work of Lammers *et al.* [24] and model the instability time t_{inst} as a function of initial orbital separation measured by a common period ratio of adjacent planets $\mathcal{P}$ for systems comprised of five Earth-mass planets of initial normalized eccentricities in $e_i/e_{cross} \in \{0.00,\ 0.25,\ 0.50,\ 0.75\}$. Our models of instability times for each normalized eccentricity are shown in Figure 7, with our results for normalized eccentricities in $e_i/e_{cross} \in \{0.00,\ 0.25,\ 0.50\}$ compared to those of Lammers *et al.* in [24].

We were also able to examine how semi-major axis a and orbital eccentricity e of each planet changes over the duration of the integrations for systems comprised of five Earth-mass planets, ten Earth-mass planets, and ten Jupiter-mass planets with a normalized eccentricity of $e_i/e_{cross} = 0.00$. Examples of our plots of a and e as a function of time for these systems are shown in Figures 8, 9, 10, 12, and 13.

Drawing parallels with the system TRAPPIST-1, where at least seven planets with sizes and masses similar to those of Earth revolve around a Jupiter-sized central star [30], our

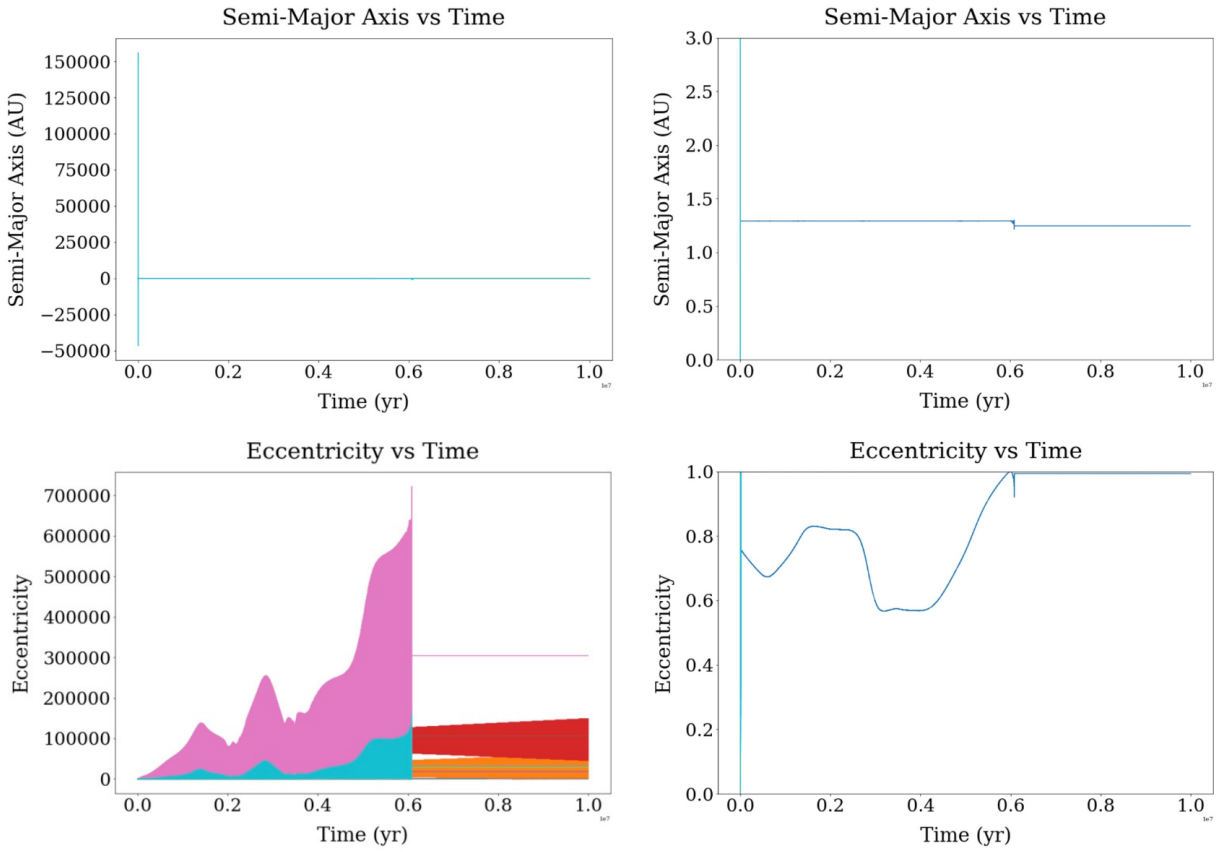

Figure 13: Semi-major axis a versus time (top row) and orbital eccentricity versus time (bottom row) for a simulation consisting of ten Jupiter-mass planets with initial orbital separation following a common period ratio $\mathcal{P} = 1.60$. An enlarged view of each plot is provided (right column).

simulations for systems of ten Earth-mass planets provide relevant context. Our observation that only one planet remains in some simulations of these systems suggests that most planets in TRAPPIST-1 will also be ejected.

Our study contributes to the ongoing exploration of compact multi-planet system evolution and stability. A potential avenue for future study includes extending our existing simulations to longer timescales, past 10^7 P_1. Such simulations would provide deeper insights into the enduring evolution of these compact systems. An example of a system that would benefit from integration on a longer timescale is one comprised of five Earth-mass planets with initial orbital separation measured by a period ratio $\mathcal{P} = 1.14$. Our results for this simulation are shown in Figure 9, where the eccentricities of the two remaining planets in the system do not appear to be stabilized by 10^7 P_1. Another potential direction of future research is to perform additional simulations of systems comprised of more planets ($N > 10$) and perhaps systems comprised of both Earth-like and Jupiter-like planets. Additionally, future research could explore the dynamics and chaos inherent in these systems and their effects on their long-term stability, as our study did not consider these factors.

$\mathcal{P}$	Stabilized a (in AU)	Stabilized e
1.20	0.66	0.4
[1]1.40	1.1	n/a
1.55	0.72	0.7
[2]1.60	1.25	0.9935
1.65	0.57	0.8
[3]1.75	1.5	0.1
1.90	0.87	0.32
[3]1.95	0.75	0.4

Figure 14: The stabilized semi-major axis a and orbital eccentricity e of the singular remaining planet in simulations of systems consisting of ten Jupiter-mass planets with initial orbital separation following period ratios $\mathcal{P} \in \{1.20,\ 1.40,\ 1.55,\ 1.60,\ 1.65,\ 1.75,\ 1.90,\ 1.95\}$. [1]The eccentricity does not stabilize to a constant value nor oscillate about a value. [2]The semi-major axis and eccentricity stabilize to the values listed after a small nudge that occurs at $t \sim 6 \cdot 10^6$ years. [3]The eccentricity oscillates about the value listed.

References

[1] W. J. Borucki *et al.*, *Kepler Planet-Detection Mission: Introduction and First Results*, Science **327**, 977 (2010).

[2] D. A. Caldwell *et al.*, *INSTRUMENT PERFORMANCE IN KEPLER's FIRST MONTHS*, ApJ Letters **713**, L92 (2010).

[3] D. C. Fabrycky *et al.*, *Architecture of Kepler's Multi-transiting Systems. II. New Investigations with Twice as Many Candidates*, ApJ **790** (2014).

[4] J. J. Lissauer *et al.*, *Validation of kepler's multiple planet candidates. II. refined statistical framework and descriptions of systems of special interest*, ApJ **784**, 44 (2014).

[5] J. F. Rowe *et al.*, *Validation of Kepler's Multiple Planet Candidates. III. Light Curve Analysis and Announcement of Hundreds of New Multi-planet Systems*, ApJ **784** (2014).

[6] J. Lissauer *et al.*, *ARCHITECTURE AND DYNAMICS OF KEPLER'S CANDIDATE MULTIPLE TRANSITING PLANET SYSTEMS*, ApJ Supplement **197** (2011).

[7] J. Lissauer *et al.*, *A closely packed system of low-mass, low-density planets transiting Kepler-11*, Nature **470**, 53 (2011).

[8] J. J. Lissauer *et al.*, *ALMOST ALL OF KEPLER'S MULTIPLE-PLANET CANDIDATES ARE PLANETS*, ApJ **750**, 112 (2012).

[9] J. J. Swift *et al.*, *CHARACTERIZING THE COOL KOIs. IV. KEPLER-32 AS A PROTOTYPE FOR THE FORMATION OF COMPACT PLANETARY SYSTEMS THROUGHOUT THE GALAXY*, ApJ **764**, 105 (2013).

[10] M. G. MacDonald *et al.*, *A DYNAMICAL ANALYSIS OF THE KEPLER-80 SYSTEM OF FIVE TRANSITING PLANETS*, The Astronomical Journal **152**, 105 (2016).

[11] T. L. Campante *et al.*, *An ancient extrasolar system with five sub-Earth-size planets*, ApJ **799**, 170 (2015).

[12] G. W. Hill, *Researches in the Lunar Theory*, American Journal of Mathematics **1**, 245 (1878).

[13] M. Henon and J. M. Petit, *Series Expansions for Encounter-Type Solutions of Hill's Problem*, Celestial Mechanics **38**, 67 (1986).

[14] J. E. Chambers, G. W. Wetherill, and A. P. Boss, *The Stability of Multi-Planet Systems*, Icarus **119**, 261 (1996).

[15] C. Marchal and G. Bozis, *Hill Stability and Distance Curves for the General Three-Body Problem*, Celestial Mechanics **26**, 311 (1982).

[16] B. Gladman, *Dynamics of Systems of Two Close Planets*, Icarus **106**, 247 (1993).

[17] D. Souami, J. Cresson, C. Biernacki, and F. Pierret, *On the local and global properties of the gravitational spheres of influence*, MNRAS **496**, 4287–4297 (2020).

[18] S. J. Morrison and K. M. Kratter, *Orbital Stability of Multi-planet Systems: Behavior at High Masses*, ApJ **823** (2016).

[19] B. Ryden and B. M. Peterson, *Foundations of Astrophysics* (Pearson Education, Inc., 2010).

[20] B. Pu and Y. Wu, *Spacing of Kepler Planets: Sculpting by Dynamical Instability*, ApJ **807** (2015).

[21] Y. Wang *et al.*, *The influence of inclinations on the dynamical stability of multi-planet systems*, MNRAS **490** (2019).

[22] A. Smith and J. Lissauer, *Orbital stability of systems of closely-spaced planets*, Icarus **201** (2009).

[23] A. Obertas, C. Van Laerhoven, and D. Tamayo, *The stability of tightly-packed, evenly-spaced systems of Earth-mass planets orbiting a Sun-like star*, Icarus **293**, 52 (2017).

[24] C. Lammers, S. Hadden, and N. Murray, *The instability mechanism of compact multi-planet systems*, arXiv (2024).

[25] H. Rein and S.-F. Liu, *REBOUND: An open-source multi-purpose N-body code for collisional dynamics*, Astronomy & Astrophysics **537** (2011).

[26] `REBOUND` Documentation. https://rebound.readthedocs.io/en/latest/.

[27] H. Rein and D. S. Spiegel, *IAS15: A fast, adaptive, high-order integrator for gravitational dynamics, accurate to machine precision over a billion orbits*, MNRAS (2014).

[28] H. Rein and D. Tamayo, *WHFast: A fast and unbiased implementation of a symplectic Wisdom-Holman integrator for long term gravitational simulations*, MNRAS (2015).

[29] H. Rein *et al.*, *Hybrid symplectic integrators for planetary dynamics*, MNRAS **485**, 5490 (2019).

[30] M. Gillion *et al.*, *Seven temperate terrestrial planets around the nearby ultracool dwarf star TRAPPIST-1*, Nature **542**, 456 (2017).